

RESEARCH

Open Access



# Pullout Behaviour of Different Types of Steel Fibres Embedded in Magnesium Phosphate Cementitious Matrix

Hu Feng<sup>1\*</sup> , M. Neaz Sheikh<sup>2</sup>, Muhammad N. S. Hadi<sup>2</sup>, Lu Feng<sup>3</sup>, Danying Gao<sup>1</sup> and Jun Zhao<sup>1</sup>

## Abstract

A series of pullout tests were conducted to investigate the interface bond properties of seven types of steel fibres embedded in the magnesium phosphate cementitious matrix. The micromorphology of the interface transition zone between MPC and different types of fibres was examined by scanning electron microscope. Test results showed that smaller diameter steel fibres with brass coating surface achieved higher average bond strength, higher pullout energy per unit volume and a higher ratio of material use. The end hook deformation provided the mechanical bond locally whereas the deformation along the length of fibre provided the mechanical bond distributed along the fibre. The failure mode and group effect of steel fibres were also investigated and reported.

**Keywords:** steel fibre, pullout, magnesium phosphate cement, failure mode, group effect

## 1 Introduction

Magnesium phosphate cement (MPC) was developed as a building material in the 1970s (Sugama and Kukacka 1983; Abdelrazig and Sharp 1985). It is generally prepared from calcined magnesia, phosphate and retarder. The major reaction occurs between magnesia and phosphate. The phosphate salts usually include ammonium dihydrogen phosphate ( $\text{NH}_4\text{H}_2\text{PO}_4$ ), potassium dihydrogen phosphate ( $\text{KH}_2\text{PO}_4$ ) and sodium dihydrogen phosphate ( $\text{NaH}_2\text{PO}_4$ ) (Abdelrazig et al. 1988; Yang and Wu 1999; Hall et al. 2001). The MPC has been used for fast repair of structures including industrial floors, highways, bridge decks, road pavement and airport runways due to its excellent engineering properties (Yang et al. 2000). The excellent engineering properties include high early strength, low shrinkage, strong bonding, favourable durability, and ability to set and harden at temperatures as low as  $-20\text{ }^\circ\text{C}$  (Yang and Wu 1999; Roy 1987; Yang et al. 2000, 2002; Abdelrazig et al. 1989). However, the MPC-based composites are typically brittle in nature

with an inherent weakness in resisting tension. They are more brittle than ordinary Portland cement (OPC) based composites because of the presence of a high volume of cementitious compounds (Ezeldin and Balaguru 1992). It has been widely recognized that the brittle behaviour of the cement-based materials can be significantly improved by the addition of discontinuous fibres (Shannag et al. 1997). Some studies found that the addition of the proper type and amount of fibres into MPC-based matrix led to composites with deflection hardening or elastic-plastic behaviour in bending (Péra and Ambroise 1998). The steel fibre is widely used for improving the strength, ductility and toughness of brittle cementitious composites due to its ease of applications and high efficiency. The tensile tests revealed a better chemical bonding of steel fibre with MPC-based matrix compared to accelerated calcium aluminate (Frantzis and Baggott 2000, 2003). The addition of the micro steel fibre significantly improved the compressive strength, flexural strength, flexural toughness and flexural ductility of MPC-based composites (Feng et al. 2018).

The improvement of the strength or toughness of the composite is largely attributed to the bond between the fibre and the matrix. The fibre-matrix interface bond strongly affects the ability of fibres to

\*Correspondence: fenghu@zzu.edu.cn

<sup>1</sup> School of Civil Engineering, Zhengzhou University, Zhengzhou, Henan 450001, China

Full list of author information is available at the end of the article  
Journal information: ISSN 1976-0485 / eISSN 2234-1315

stabilize crack propagations in the matrix. The interface bond between the steel fibre and matrix consists of the physicochemical bond and mechanical bond contributions. The physicochemical bonding is significantly influenced by the surface properties of the fibre and the packing density of cementitious matrix. The mechanical bond contribution is significantly influenced by the geometric deformations of the fibre and the compressive strength of the matrix. The ends deformations of the fibre provide the mechanical bond contribution locally, whereas the deformations along the fibre length (e.g. the indented, twisted, or crimped fibres) provide the mechanical bonding contribution distributed along the fibre length (Wille and Naaman 2012). The pullout test of the fibre from the cementitious matrix is generally used to investigate the bond properties of the interface of the fibre–matrix (Shannag et al. 1997). The factors that influence the mechanical properties of fibre-reinforced-cementitious-composites are the length and diameter of the fibre (Naaman and Shah 1976; Betterman et al. 1995), fibre shape (Ramakrishnan et al. 1980; Banthia and Trottier 1995), volume fraction (Rossi and Harrouche 1990), interface strength of the fibre–matrix (Chan and Chu 2004), surface properties of the fibre (Li et al. 1990; Peled et al. 1992), fibre distribution and combination (Ohama et al. 1985; Banthia and Sheng 1990; Stähli et al. 2008). The effects of these factors on the mechanical properties can be experimentally investigated by the pullout test of the fibre.

The reinforcing effect of the steel fibre on the cementitious composites is influenced significantly by the type and properties of the steel fibre, such as tensile strength, surface roughness, geometric deformation and diameter. Some studies indicated that the physicochemical bond between the steel fibre and MPC-based matrix was much better than the physicochemical bond between the steel fibre and OPC-based matrices (Feng et al. 2018). However, the effect of the type of the fibre on the bond properties between the steel fibre and MPC-based matrix is yet to be fully investigated.

In this study, the pullout tests of seven types of steel fibres embedded in the MPC-based matrix were carried out. The effects of fibre types on the pullout behaviour were investigated. The group effect of steel fibre on the pullout behaviour was also explored. The results obtained from this investigation are important for better understanding the role of steel fibre in improving the strength and toughness of MPC-based composites. Also, the results are helpful in selecting suitable fibres to efficiently reinforce MPC-based composites.

## 2 Experimental Program

### 2.1 Materials and Mixture Proportions

The magnesium phosphate cement (MPC) consisted of magnesium oxide (MgO), potassium dihydrogen phosphate ( $\text{KH}_2\text{PO}_4$ ) and retarder. The magnesium oxide (MgO) in the form of calcined magnesia powder was provided by Zhengyang Casting Material Company of Xinmi, Henan, China (Xinmi et al. 2018). The oxide composition of calcined magnesia powder is listed in Table 1 (Xinmi et al. 2018). The potassium dihydrogen phosphate (industrial-grade,  $\text{KH}_2\text{PO}_4$ ) with a particle size of 180–385  $\mu\text{m}$ , a purity of 96%, and relative density of 2.338 was provided by Weitong Chemical Co., Ltd of Wujiang, Jiangsu, China (2018). The retarder was prepared from mixing the borax ( $\text{Na}_2\text{B}_4\text{O}_7 \cdot 10\text{H}_2\text{O}$ ), disodium hydrogen phosphate dodecahydrate ( $\text{Na}_2\text{HPO}_4 \cdot 12\text{H}_2\text{O}$ ) and calcium chloride ( $\text{CaCl}_2$ ). The borax (industrial-grade,  $\text{Na}_2\text{B}_4\text{O}_7 \cdot 10\text{H}_2\text{O}$ ) with a particle size of 80–220  $\mu\text{m}$ , and a purity of 95%, was provided by Banda Technology Co., Ltd. of Liaoning, China (2018). The  $\text{CaCl}_2$  (analytic grade, purity of 96%) and the  $\text{Na}_2\text{HPO}_4 \cdot 12\text{H}_2\text{O}$  (analytic grade, purity of 99%) were provided by Kermel Chemical Reagent Co., Ltd. of Tianjin, China (2018). The natural river sand with a fineness modulus of 2.06 and tap water were used in this study.

The mixture proportion of MPC-based matrix is shown in Table 2. The mass ratios of sand to MPC and water to MPC are 0.8 and 0.14, respectively. The MPC consists of the magnesia and potassium dihydrogen phosphate. The mole ratio of magnesia (MgO) to potassium dihydrogen phosphate ( $\text{KH}_2\text{PO}_4$ ) in cement is 4.0. The retarder consists of borax ( $\text{Na}_2\text{B}_4\text{O}_7 \cdot 10\text{H}_2\text{O}$ ), disodium hydrogen phosphate dodecahydrate ( $\text{Na}_2\text{HPO}_4 \cdot 12\text{H}_2\text{O}$ ) and calcium chloride ( $\text{CaCl}_2$ ). The mass ratio of B,  $\text{Na}_2\text{HPO}_4 \cdot 12\text{H}_2\text{O}$  and  $\text{CaCl}_2$  in the retarder is 1:3:1. The dosage of the retarder is 9.0% of magnesia by mass.

Seven types of steel fibres were investigated in this study: S-1, S-2, H-1, H-2, R-H, C-A and I-A. Different types of steel fibres grouped according to their bond characteristics are shown in Fig. 1. The S-1 and S-2 fibres (smooth surface and round section) are straight. The H-1 and H-2 fibres (smooth surface and round section) are hooked at the ends. The R-H fibre (one side roughened and flat section) are hooked at the ends. The C-A and I-A fibres are crimped and indented along the length of fibre, respectively. The surface micro-morphology of the fibres is presented in Fig. 2. The material

**Table 1 Oxide composition of calcined magnesia (Xinmi et al. 2018).**

Composition	MgO	$\text{Fe}_2\text{O}_3$	$\text{SiO}_2$	CaO	Others
Mass fraction of the sample (%)	92.53	0.87	3.1	1.6	1.9

**Table 2 Mixture proportion of MPC-based matrix.**

Sand to MPC mass ratio	Water to MPC mass ratio	MgO to $\text{KH}_2\text{PO}_3$ mol ratio	Retarder
0.8	0.14	4	9.0%

The MPC consists of magnesium oxide (MgO) and potassium dihydrogen phosphate ( $\text{KH}_2\text{PO}_4$ ). The retarder dosage is 9.0% of MgO by mass.

and surface of fibre S-1 are the same with that of fibre H-1. The material and surface of fibre S-2 are the same with that of fibre H-2. The properties of steel fibre provided by the manufacturers (Shanghai Realstrong Steel Fibre Co., Ltd. 2018; Bekaert China Co., Ltd. 2018; Shanghai Harex Steel Fiber Technology Co., Ltd. 2018; Zhitai Steel Fiber Co., Ltd. 2018; Zhengzhou YuJian Steel Fiber Co., Ltd. 2018) are reported in Table 3. The equivalent circular cross-sectional area of the fibre was calculated by dividing the volume of the individual fibre by its length. The equivalent diameter was then calculated from the equivalent cross-sectional area.

**2.2 Specimen Preparation**

According to the recommendation in ASTM C109M-13, the prism specimens (50 mm × 50 mm × 50 mm) were used to test the compressive strength (ASTM C109/C109M-16a 2016). According to recommendation in JCI SF-8, the dog-bone shaped specimens were adopted in the pullout test of steel fibres embedded in MPC-based matrices (JCI SF-8 2002). The number of various fibres in each dog-bone shaped specimen is shown in the last column of Table 3. The pullout tests of H-2 fibres with varying spacing and numbers were carried out to investigate the group effect of the steel fibres on the pullout behaviour. The equivalent diameters of R-H, I-A and C-A fibres are significantly larger bigger than the equivalent diameters of the other fibres. The thickness of the matrix surrounding R-H, I-A and C-A fibres are significantly smaller than the thickness of the matrix surrounding of the other fibres. In order to avoid the break of matrix around the fibers, the Nf of R-H, I-A and C-A fibres were set to 3, 1 and 1, respectively. Figure 3 presents the specimen with four fibres. The dog-bone shaped specimen was divided into the fixed half and pullout half by

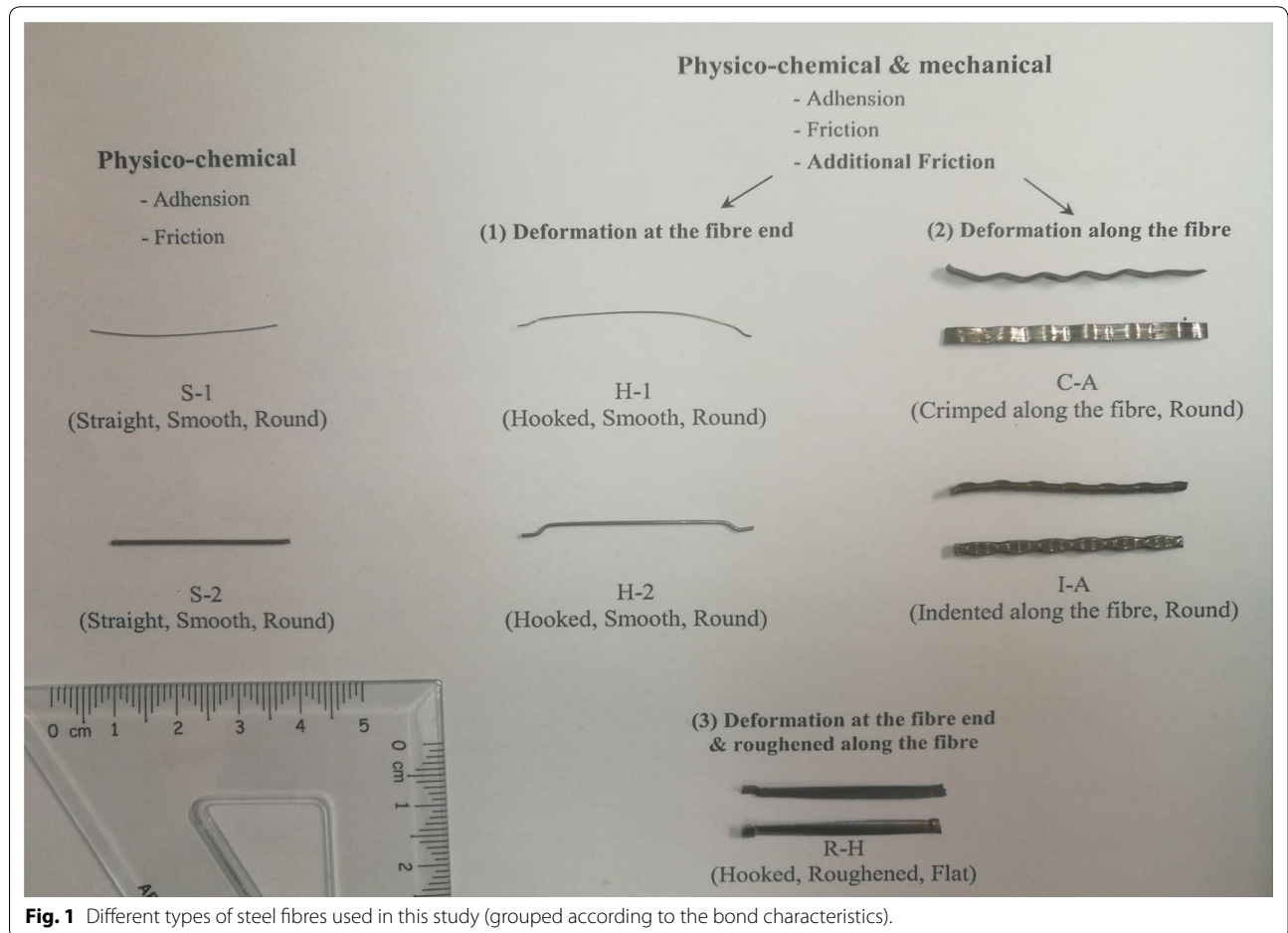


**Fig. 1** Different types of steel fibres used in this study (grouped according to the bond characteristics).

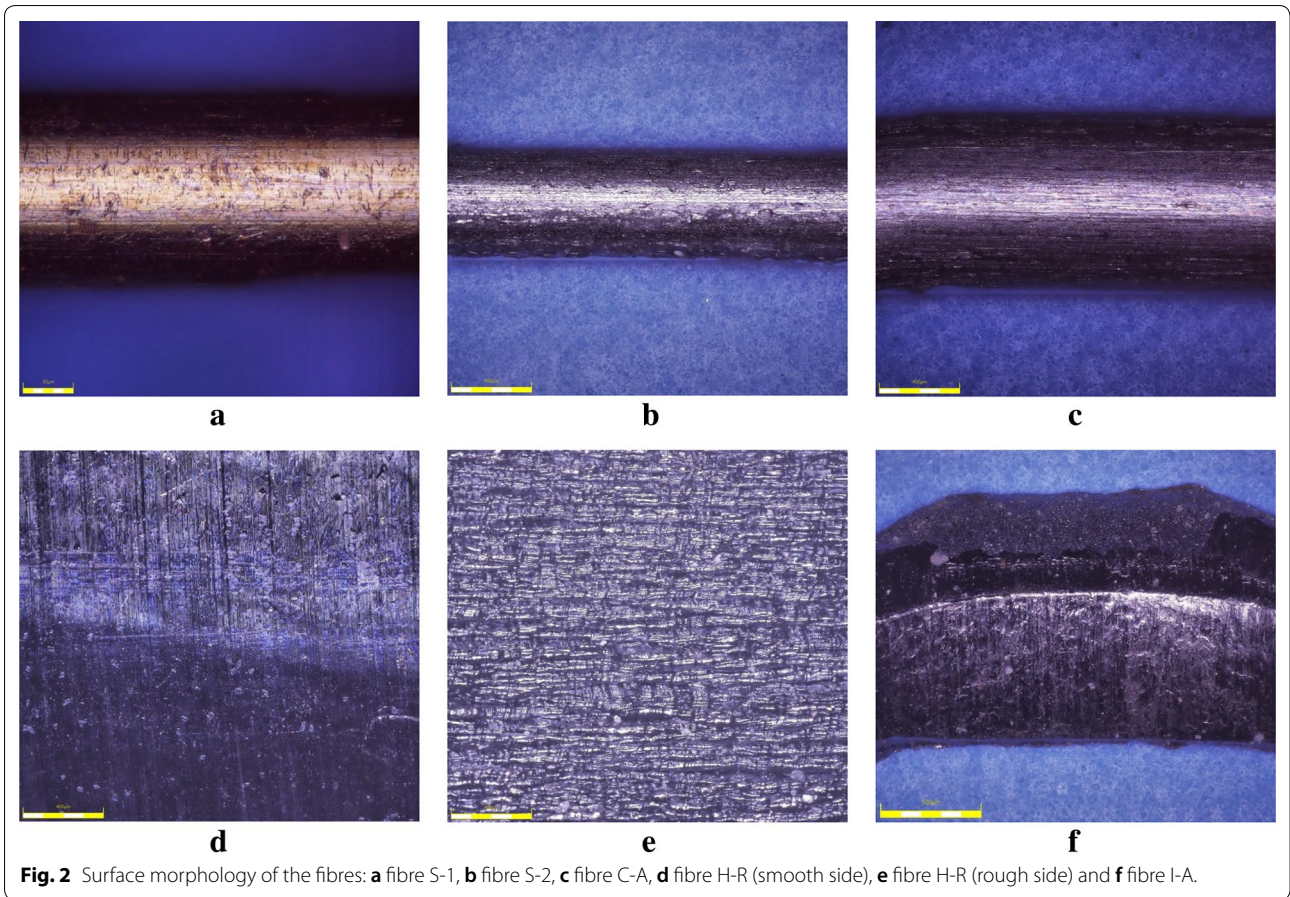
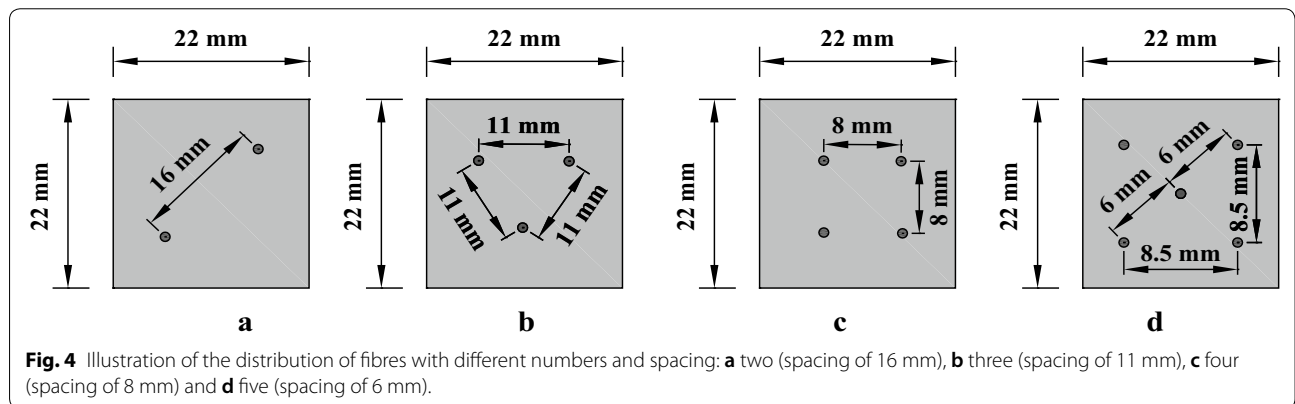
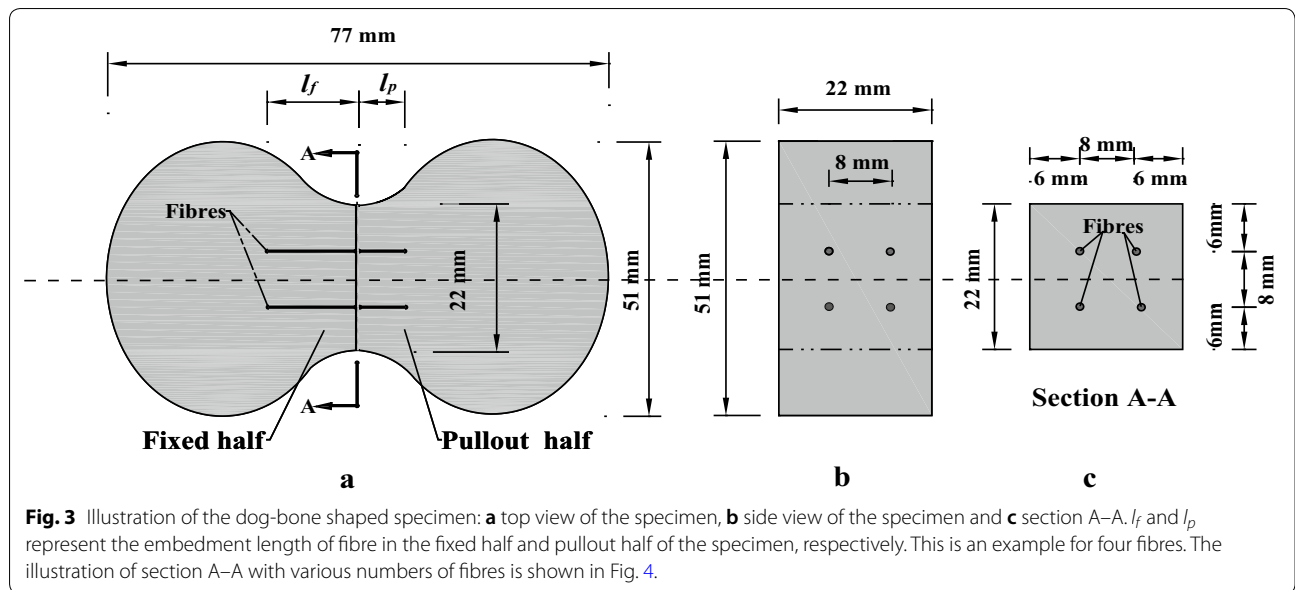


**Fig. 2** Surface morphology of the fibres: **a** fibre S-1, **b** fibre S-2, **c** fibre C-A, **d** fibre H-R (smooth side), **e** fibre H-R (rough side) and **f** fibre I-A.

**Table 3** Properties of the steel fibres (Shanghai Realstrong Steel Fibre Co., Ltd. 2018; Bekaert China Co., Ltd. 2018; Shanghai Harex Steel Fiber Technology Co., Ltd. 2018; Zhitai Steel Fiber Co., Ltd. 2018; Zhengzhou YuJian Steel Fiber Co., Ltd. 2018).

Fibre profile	Type	Length (mm)	Equivalent diameter (mm)	Tensile strength (MPa)	Shape and surface	$l_p$ (mm)	$N_f$
	S-1 (Shanghai Realstrong Steel Fibre Co., Ltd. 2018)	30	0.22	2850	Straight, smooth, round	9	4
	S-2 (Bekaert China Co., Ltd. 2018)	30	0.75	1100	Straight, smooth, round	8	4
	H-1 (Shanghai Realstrong Steel Fibre Co., Ltd. 2018)	38	0.22	2850	Hooked, smooth, round	9	4
	H-2 (Bekaert China Co., Ltd. 2018)	35	0.54	1200	Hooked, smooth, round	9	2, 3, 4, 5
	R-H (Shanghai Harex Steel Fiber Technology Co., Ltd. 2018)	32	0.91	600	Hooked, roughened, flat	9	3
	I-A (Zhitai Steel Fiber Co., Ltd. 2018)	36	1.57	800	Indented, round	11	1
	C-A (Zhengzhou YuJian Steel Fiber Co., Ltd. 2018)	40	1.26	600	Crimped, FLAT	10	1

The  $N_f$  represents the number of various fibres in each specimen of pullout tests. The  $l_p$  represents the embedment length of fibre in the pullout half of the specimen.



a partitioning board with a thickness of 1.0 mm. The two halves of the dog-bone shaped specimen were bridged by the steel fibres. The group effect of steel fibre on the pullout behaviour was investigated through to test the specimens with different numbers of the fibres. Figure 4 shows the partitioning boards (section A-A) of the specimens with different numbers of the fibres. The details of the distributions and spacing of the fibres are presented in Fig. 4.

The casting process is as follows. Firstly, the MPC paste was cast into the half of the steel mould. Secondly, the steel fibres were inserted into the MPC paste and carefully arranged to be perpendicular to the steel partitioning board. The embedded length of the fibre in the fixed half is much larger than the embedded length of the pullout fibre in the half. The steel fibres were pulled out from the pullout half during the test processing. After 2 h of casting the half, the partitioning board was

covered with the cling wrap. The cling wrap was used to separate the two halves of the specimen. Finally, the MPC paste was cast in the other half of the mould. The 50 mm × 50 mm × 50 mm prism and dog-bone shaped specimens were demolded after 1 h of casting. The specimens were then cured for 7 days in a standard curing room with an average relative humidity of 95% and an average temperature of 20 °C.

### 2.3 Test Procedure

An electronic universal machine with a capacity of 5 kN was used to test the fibre pullout behaviour. The slip between the fibre and MPC-based matrix was measured by an extensometer, as presented in Fig. 5 (JCI SF-8 2002). The loading rate was 0.5 mm slip per minute. Five specimens were tested for each group. The presented results represent the average curve or average value of the experimental data of each group with five specimens. The

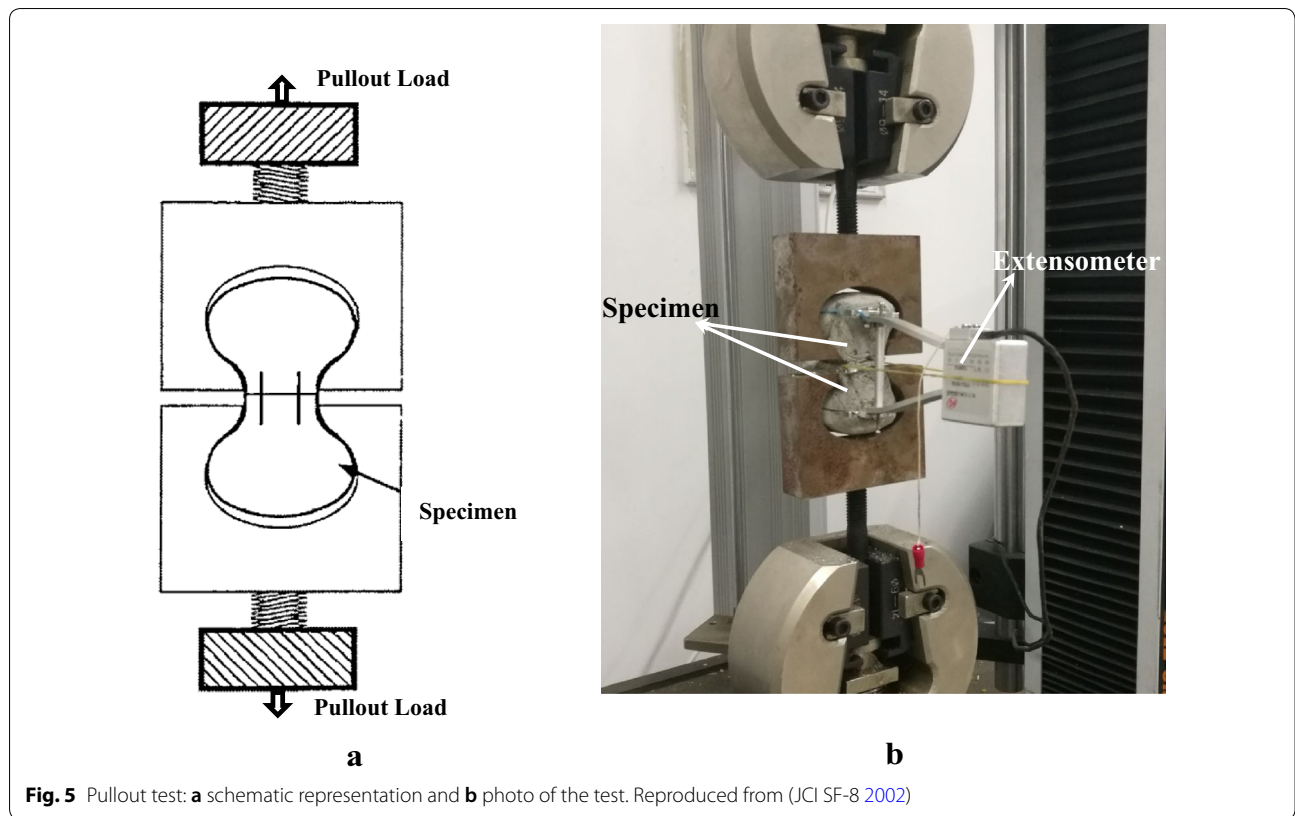


**Fig. 5** Pullout test: **a** schematic representation and **b** photo of the test. Reproduced from (JCI SF-8 2002)

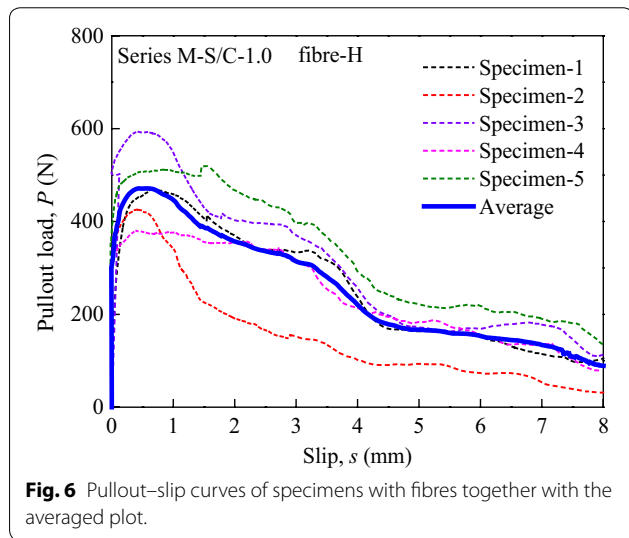


**Fig. 6** Pullout-slip curves of specimens with fibres together with the averaged plot.

presented curves of each group were got by averaging the values of the pull load at regular slip increments. Figure 6 presents the pullout-slip curves of the five individual results together with the average results for Specimen with fibre-H (Wille and Naaman 2012; Feng et al. 2018). The effects of the elastic deformations of the fibre and the specimen were neglected. The surface micro-morphology

of the fibres was examined by optical digital microscope (Olympus DSX500, Japan). The micromorphology of the interface transition zone between MPC and different types of fibres was examined by field emission scanning electron microscope (Zeiss, Auriga FIB, Germany).

**3 Evaluation Parameters of Pullout Behaviour**

Each fibre pullout test is presented by the behaviour of pullout load versus slip ( $P-s$ ), where  $P$  is the pullout load and  $s$  is the slip. The tensile stress induced in the fibre ( $\sigma_f(s)$ ) is calculated using Eq. (1).

$$\sigma_f(s) = \frac{P(s)}{A_f} = \frac{4 \times P(s)}{\pi \times d_f^2} \tag{1}$$

where  $P(s)$  is the pullout load at slips  $s$ ,  $A_f$  is the fibre cross-sectional area and  $d_f$  is the diameter of the circular fibre or the equivalent diameter of the non-circular fibre.

The pullout load at any slip  $P(s)$  divided by the surface area of the embedded portion of the fiber ( $\pi \times d_f \times (l_p - s)$ ) leads to a slip-dependent bond stress  $\tau(s)$ . The slip-dependent bond stress represents the average bond stress over the embedment length,  $(l_p - s)$ , where  $l_p$  is the initial embedment length and  $s$  is the slip during pullout. The bond stress  $\tau(s)$  can be calculated using Eq. (2).

$$\tau(s) = \frac{P(s)}{\pi \times d_f \times (l_p - s)} \tag{2}$$

To simplify the comparison between different specimens, the  $\tau_{av}$  is defined as the average bond strength according to the maximum pullout-load and the initial embedded length (Stähli et al. 2008). The  $\tau_{av}$  is calculated using Eq. (3).

$$\tau_{av} = \frac{P_{max}}{\pi \times d_f \times l_p} \tag{3}$$

where,  $P_{max}$  is the maximum pullout load.

The total pullout energy,  $W_p$ , is the integration of the area under the pullout load–slip curve. The  $W_p$  is calculated using Eq. (4).

$$W_p = \int P(s)ds \tag{4}$$

The total pullout energy is usually determined to up to 2.5 mm slip, according to the recommendation in JCI SF-8 (2002). The pullout energy per unit volume,  $W_{uv}$ , is defined as the total pullout energy divided by the volume of the embedded fibre. The  $W_{uv}$  is calculated using Eq. (5).

$$W_{uv} = \frac{W_p}{V_{fe}} \tag{5}$$

where  $V_{fe}$  is the volume of the embedded portion of the fibre. The pullout energy per unit volume,  $W_{uv}$ , is used to compare pullout energy of fibre with different embedded volume due to different cross-section area.

The high bonding strength can increase the maximum tensile stress induced in the fibre. And it can also cause a high tensile strength and flexural strength of the fibre reinforced cementitious composites. The pullout energy is regarded as the mechanical energy consumed during the fibre pullout and thus possesses a better correlation to the fracture energy of fibre reinforced cementitious composites (Helfet and Harris 1972).

#### 4 Results and Discussion

Figures 7 and 8 present the pullout load–slip curves and fibre tensile stress–slip curves, respectively, for Fibres S-1, H-1, S-2 and H-2. Figures 9 and 10 present the pullout load–slip curves and fibre tensile stress–slip curves, respectively, for Fibres R-H, I-A and C-A. Figures 11 and 12 present the average bond strength and pullout energy per unit volume, respectively, for all the fibres. The average compressive strength of MPC-based matrix is 37.4 MPa. Table 4 summarizes all the pullout parameters (the maximum pullout load, maximum fibre tensile

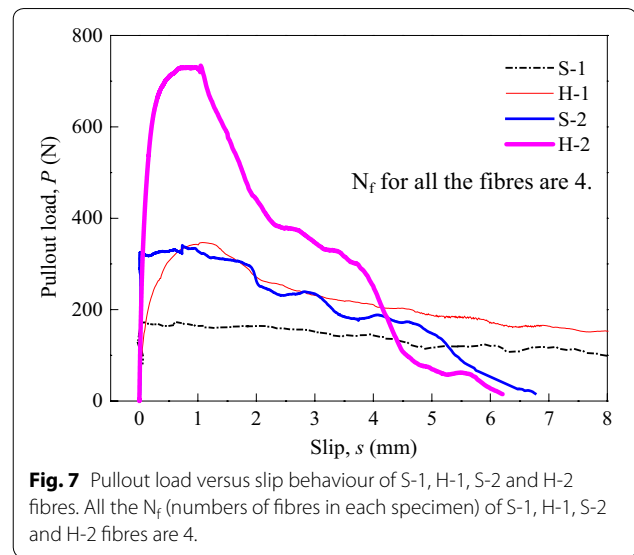


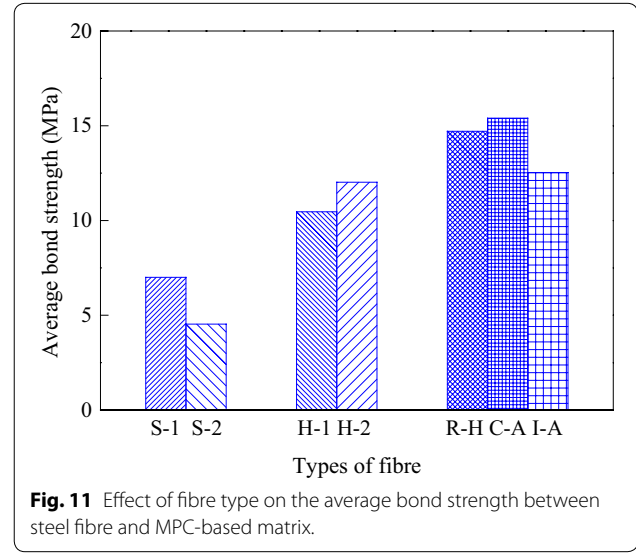
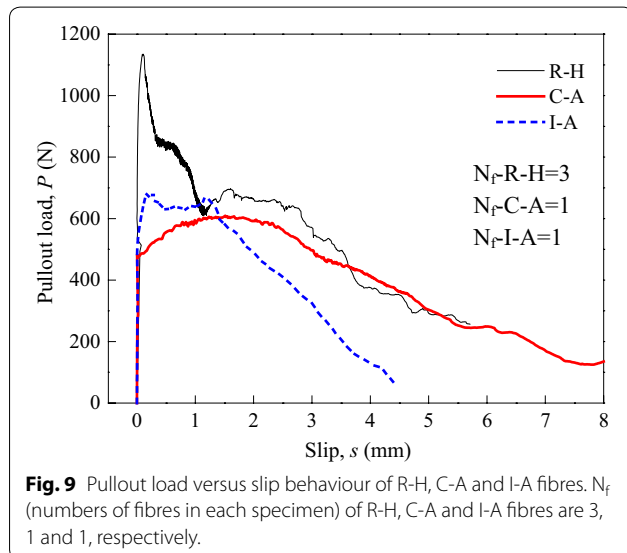
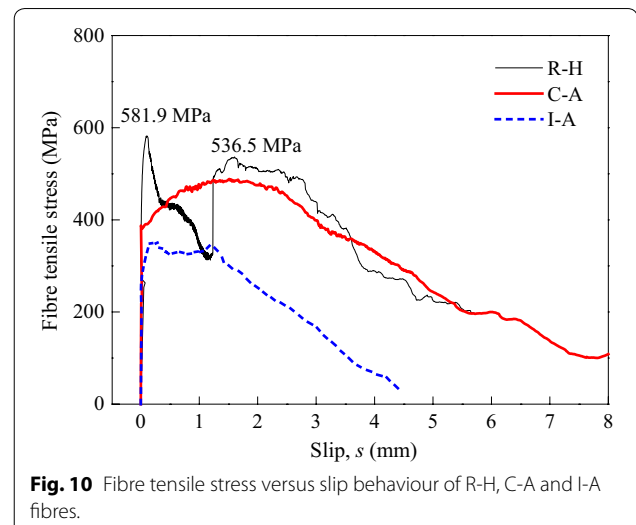
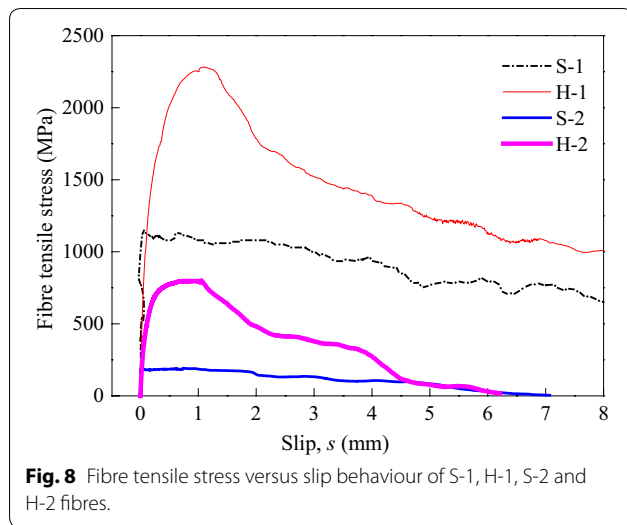
**Fig. 7** Pullout load versus slip behaviour of S-1, H-1, S-2 and H-2 fibres. All the  $N_f$  (numbers of fibres in each specimen) of S-1, H-1, S-2 and H-2 fibres are 4.

stress, average bond strength, and pullout energy per unit volume).

#### 4.1 Effect of End-Hook Deformation

As shown in Figs. 7 and 8, the H-2 fibres embedded in MPC-based matrix showed the typical pullout behaviour of hooked-end fibres embedded in OPC-based matrix, which is generally characterized by a steep increase followed by a two-step decrease of the pullout load or fibre tensile stress due to the progressive straightening of the end hook (Naaman and Najm 1991; Robins et al. 2002; Kim et al. 2008; Cunha et al. 2010). The H-1 fibres embedded in MPC-based matrix showed a similar pullout behaviour to H-2 fibres, but with only a one-step significant decrease of pullout load or fibre tensile stress with the progressive straightening of the end hook because of the smaller angle of the end-hook of H-1 fibres. After the end-hook of the H-1 and H-2 fibres was fully straightened, the pullout behaviour was similar to that of a straight fibre.

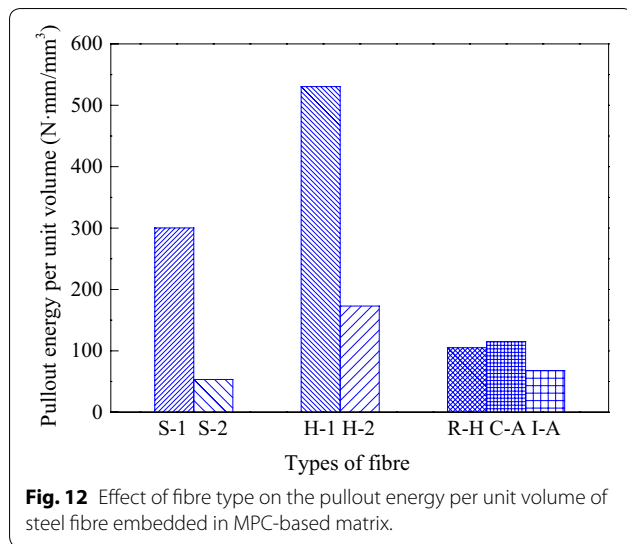
The mechanical bond contribution of deformed fibres in comparison to straight fibres can be assessed from the induced fibre tensile stress (Wille and Naaman 2012). The maximum fibre tensile stress ( $\sigma_{fmax}$ ) of 2282.5 MPa for the pulled-out of hooked-end fibres (H-1) is approximately two times the tensile stress of 1145.7 MPa achieved by the straight fibres (S-1). The maximum fibre tensile stress ( $\sigma_{fmax}$ ) of 801.4 MPa for the pulled-out of hooked-end fibres (H-2) is approximately four times the maximum fibre tensile stress of 193.1 MPa achieved by the straight fibres (S-2). The mechanical bond contribution was very significant due to the end-hook



deformation of the steel fibre. The mechanical bond contribution due to the end-hook deformation was calculated and analyzed below to compare end-hook fibres to straight fibres (H-1 to S-1 and H-2 to S-2).

The pullout resistance of a single straight fibre is predominantly controlled by the physicochemical bond properties between the matrix and fibre surface. The total bond for the straight fibres (S-1 and S-2) is mostly the physicochemical bond. The materials, diameter and surface properties of the S-1 and H-1 fibres are the same. The total bond of the S-1 fibre represents approximately the physicochemical bond contribution for the H-1 fibre. Based on the pullout tests of the S-1 fibre embedded in the same matrix, the physicochemical bond contributions for the pullout load and fibre tensile stress of the

H-1 fibre were 43.5 N and 1145.7 MPa, respectively. The maximum pullout load and fibre tensile stress for the H-1 fibre were 86.7 N and 2282.5 MPa, respectively. Thus, the mechanical bond contributions to pullout load and fibre tensile stress of the H-1 fibre were calculated as 43.2 N and 1136.8 MPa, respectively. The ratio of the mechanical bond contribution to the total bond for the H-1 fibre was 49.8%. The physicochemical bond contribution to the average bond strength of the H-2 fibre was similar to that of the S-2 fibre because of the same materials and surface of S-2 and H-2 fibres. Based on the pullout tests of the S-2 fibre embedded in the same matrix, the physicochemical bond contributions for the pullout load and fibre tensile of H-2 fibre were calculated as 68.7 N and 300.1 MPa, respectively.



The mechanical bond contributions to the pullout load and fibre tensile stress of the H-2 fibre were calculated as 114.8 N and 501.3 MPa, respectively. The ratio of the mechanical bond contribution to the total bond for the H-2 fibre was 62.6%. The mechanical bond contribution of H-2 fibre (62.6%) was more than that of H-1 fibre (49.8%) due to the bigger angle of end hook of H-2 fibre, as shown in Fig. 1. The ratio of material use is defined as the maximum tensile stress achieved through pullout  $\sigma_{fmax}$  divided by the material tensile strength  $f_u$  (Wille and Naaman 2012). The ratio of material use of H-1 fibre (80.1%) was twice that of the S-1 fibre (40.2%). The ratio of material use of H-2 fibre (66.8%) was 3.8 times that of the S-2 fibre (17.6%). The end-hook deformation of the steel fibre significantly improved the ratio of material use.

#### 4.2 Effect of Diameter and Surface Coating of Fibres

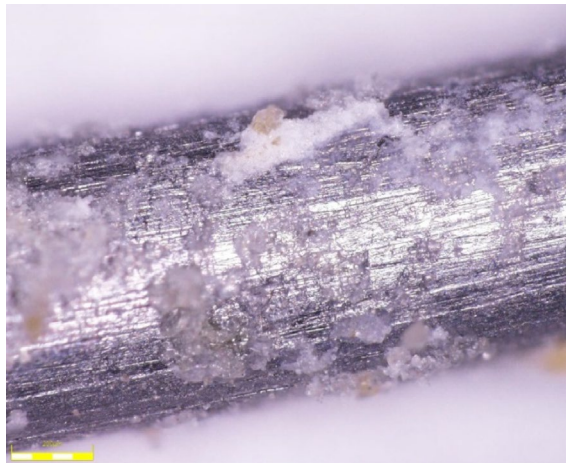
Comparing the pullout behaviours of the fibres with different diameter and surface coating (S-1 to S-2 and H-1

to H-2), the effects of diameter and surface coating of fibres are discussed herein. During the pullout process, the small diameter steel fibre stresses the matrix less than the larger diameter steel fibre (Wille and Naaman 2012). Hence, the risk of failure of the matrix surrounding the fibres with a small diameter is reduced. Additionally, the strength and Young’s modulus of the brass are usually smaller than those of the steel. The surface of S-1 fibre with a brass coating is easier to be damaged during the pullout process. The damaging and scratching of the surface of S-1 fibre was found from the micro-morphology examination by optical digital microscope (Fig. 13). The damaging and scratching of the surface increase the surface roughness and thus the frictional coefficient. The effect of the lower risk of the failure of the matrix surrounding the fibres and the more serious damage of the fibre surface during the pullout process makes fibre S-1 to possess higher bond strength. The maximum fibre tensile stress of 1145.7 MPa in S-1 fibre was 5.9 times the maximum fibre tensile stress of 193.1 MPa in S-2 fibre during the pullout process from the same matrix, as shown in Fig. 8. The average bond strength of S-1 fibre with the smaller diameter and brass coating was 1.6 times the average bond strength of S-2 fibre, as shown in Fig. 11. The pullout energy per unit volume of S-1 fibre was 5.6 times the pullout energy per unit volume of S-2 fibre, as shown in Fig. 12. The S-1 fibres showed a more efficient crack-bridging behaviour for the fibre-reinforced composite. These two effects were also effective for the physicochemical bond contribution of H-1 fibre (with a  $d_f = 0.22$  mm and coating surface) and H-2 fibre (with a  $d_f = 0.54$  mm). The H-1 fibre showed a more efficient crack-bridging behaviour for the fibre-reinforced composite than H-2 fibre. The maximum fibre tensile stress of 2282.5 MPa in H-1 fibre was 2.8 times the maximum fibre tensile stress of 801.4 MPa in H-2 fibre during the pullout process from the same matrix. The pullout energy per unit volume of H-1 fibre was 2.9 times the pullout energy per unit

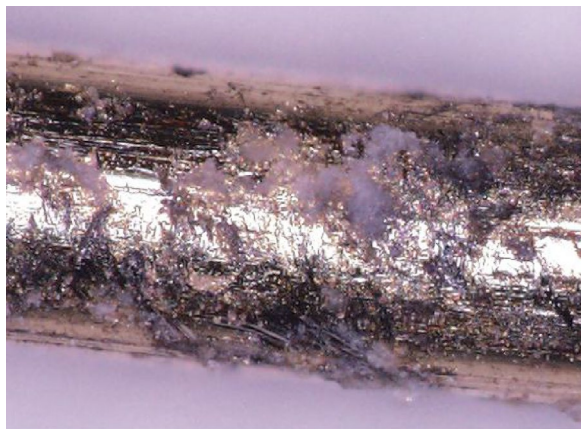
**Table 4** Pullout parameters derived from test results for different fibres.

Group	Compressive strength of matrix (MPa)	Maximum pullout load (N)	Maximum fibre tensile stress (MPa)	Average bond strength (MPa)	Pullout energy per unit volume (N mm/mm <sup>3</sup> )
S-1	37.4	174.1	1145.7	7.0	300.2
S-2		341.1	193.1	4.5	53.3
H-1		346.9	2282.5	10.5	530.5
H-2		733.8	801.4	12.0	173.1
R-H		1134.8	581.9	14.7	105.1
I-A		679.6	351.2	12.5	68.0
C-A		609.1	488.8	15.0	115.1

The reported values are the average values of the test results.



**a** Straight fibre S-2



**b** Straight fibre S-1 with brass coating

**Fig. 13** Micro-morphology of fibre surface pulled out from MPC-based matrix (examined by optical digital microscope).



**Fig. 14** Photo of the failed specimen of R-H fibre.

volume of H-2 fibre, as shown in Fig. 12. However, due to the bigger angle of the end hook (Fig. 1) which caused more mechanical bond contribution, the average bond

strength of H-2 fibre was slightly more than the average bond strength of H-1 fibre.

It is noted that for the same volume fraction of fibres, the number of small-diameter fibres is significantly larger than that of the larger-diameter fibres. The group effect during pullout may reduce the fibre efficiency above.

### 4.3 Effect of Deformations Along Fibre Length and Rough Surface

Unlike the hooked-end fibres (H-1 and H-2), for which the pullout load dropped significantly after the end hook straightened up, the crimped fibres (C-A) maintained a high pullout load resistance up to very high slips. The pullout load of C-A fibre decreased steadily but slowly with an increase in the slip. The ratio of material use of C-A fibre defined in Sect. 4.2 is 81.5%, which is similar to that of hooked-end fibre H-1 and more than that of hooked-end fibre H-2. The physicochemical bond contribution is predominantly determined by the cementitious matrix packing density and the fibre surface properties (Wille and Naaman 2012). The surface of C-A and S-2 fibres are similar, as well as the matrices surrounding C-A and S-2 fibres. Thus, the physicochemical bond contribution for pullout load of the C-A fibre can be estimated based on the average bond strength of the straight S-2 fibre, which only possesses physicochemical bond. The physicochemical bond contribution to the pullout load of C-A fibre was calculated as approximately 178.0 N and the mechanical bond contribution was then calculated as approximately 431.1 N. The ratios of the physicochemical and mechanical bond contributions to the total bond were 29.2% and 70.8%, respectively.

The surface of the rough side of R-H fibre is significantly rougher compared to H-1 and H-2 fibres, as shown in Fig. 2a, b and e. Due to the surface roughness and end hook, the average bond strength of the R-H fibre is significantly more than that of the hooked-end fibres (H-1 and H-2) and is similar to that of the crimped fibre (C-A), as shown in Fig. 11. It is noted that one of the three R-H fibres embedded in the matrix failed during the pullout test, as shown in Fig. 14. The average maximum fibre tensile stress of the R-H fibre was 581.9 MPa, which was close to the fiber tensile strength. The average ratio of material use of three fibres was approximately 97%. The distribution of the pullout load for the three fibres was uneven and the fibre tensile stresses in the three fibres were not the same. Hence, one of the R-H fibres achieved the tensile strength and then failed. As shown in Fig. 9, the pullout load of the R-H fibres dropped sharply due to the failure of one fibre. However, the pullout load was maintained by approximately 61.5%, which was provided by the remaining two fibres. As shown in Fig. 10, the maximum average fibre tensile stress (536.5 MPa) in the

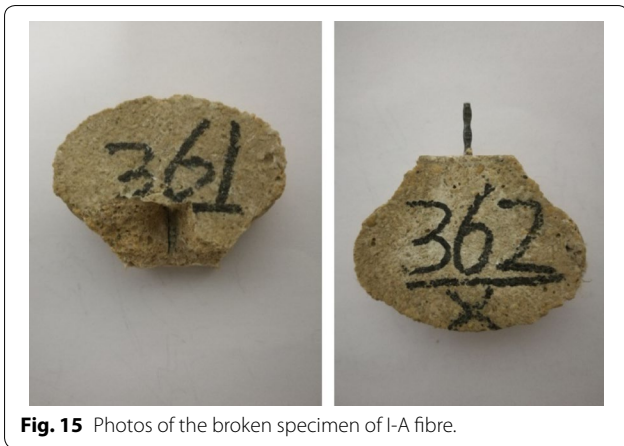


**Fig. 15** Photos of the broken specimen of I-A fibre.

remaining two fibres was less than the maximum average fibre tensile stress (581.9 MPa) in the three fibres before one of the fibres failed. Hence, the two remaining fibres did not fail and finally pulled out from the matrix. However, in order to ensure the entire fibres pullout from the MPC-matrix (avoid fiber failing), the embed length of the fibers should be reduced.

During the pullout process of the indented fibre (I-A), the matrix surrounded the fibre split at a slip of approximate 1.2 mm, then the pullout load dropped steeply followed by the fracture of the pullout half of the specimen at a slip of approximate 4.5 mm, as shown in Fig. 9. The stress distribution was more uneven, which was caused by the indentation deformation of I-A fibre. The transverse tensile stress to the matrix surrounded the indented fibre (I-A) during pullout test was very significant, which

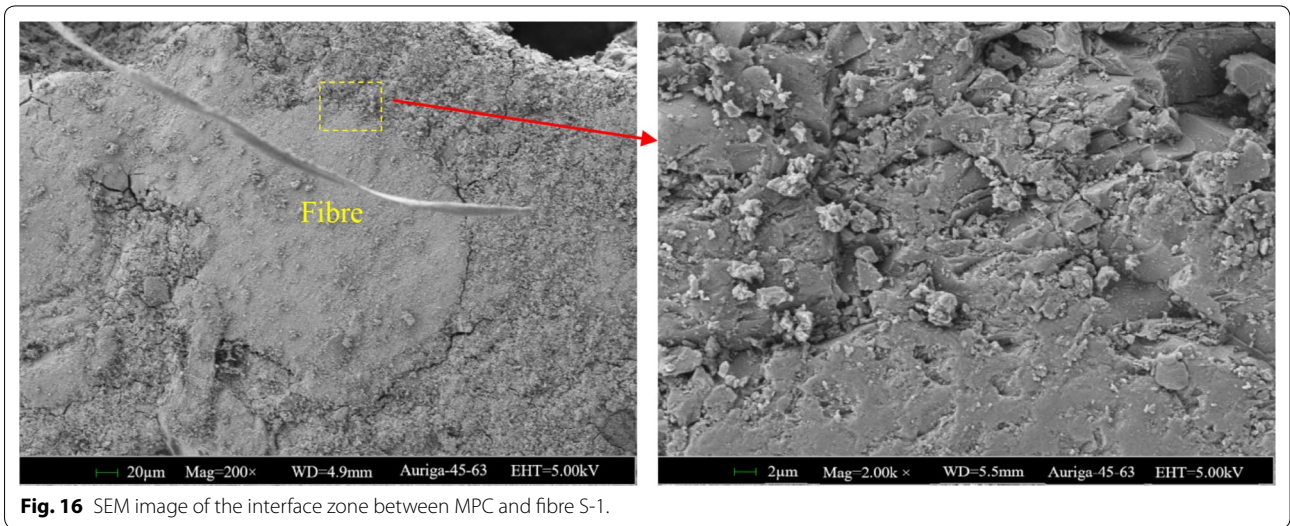


**Fig. 16** SEM image of the interface zone between MPC and fibre S-1.

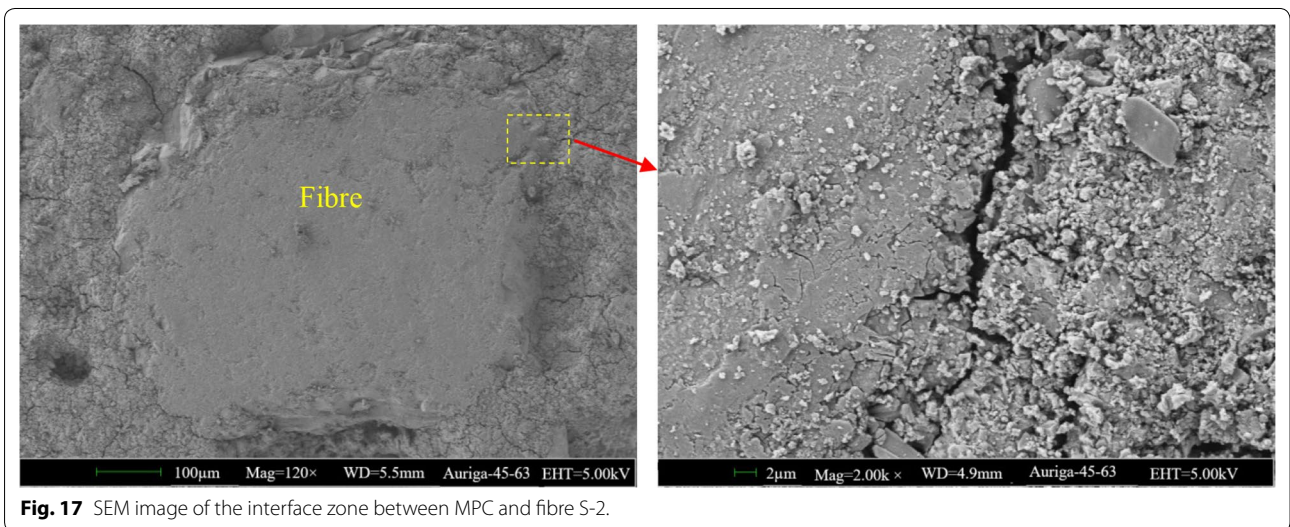
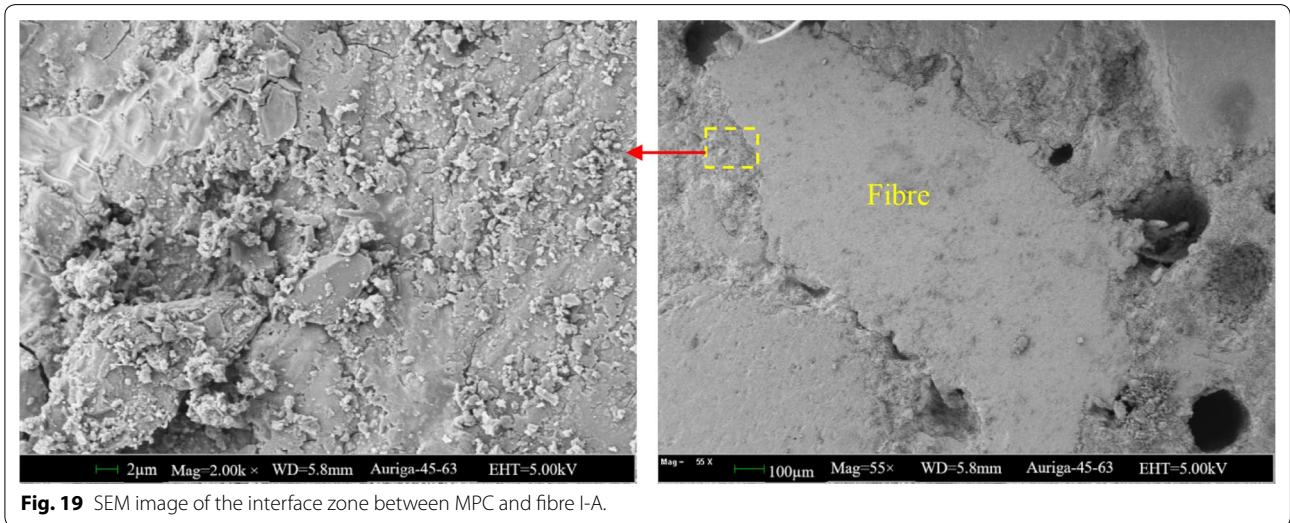
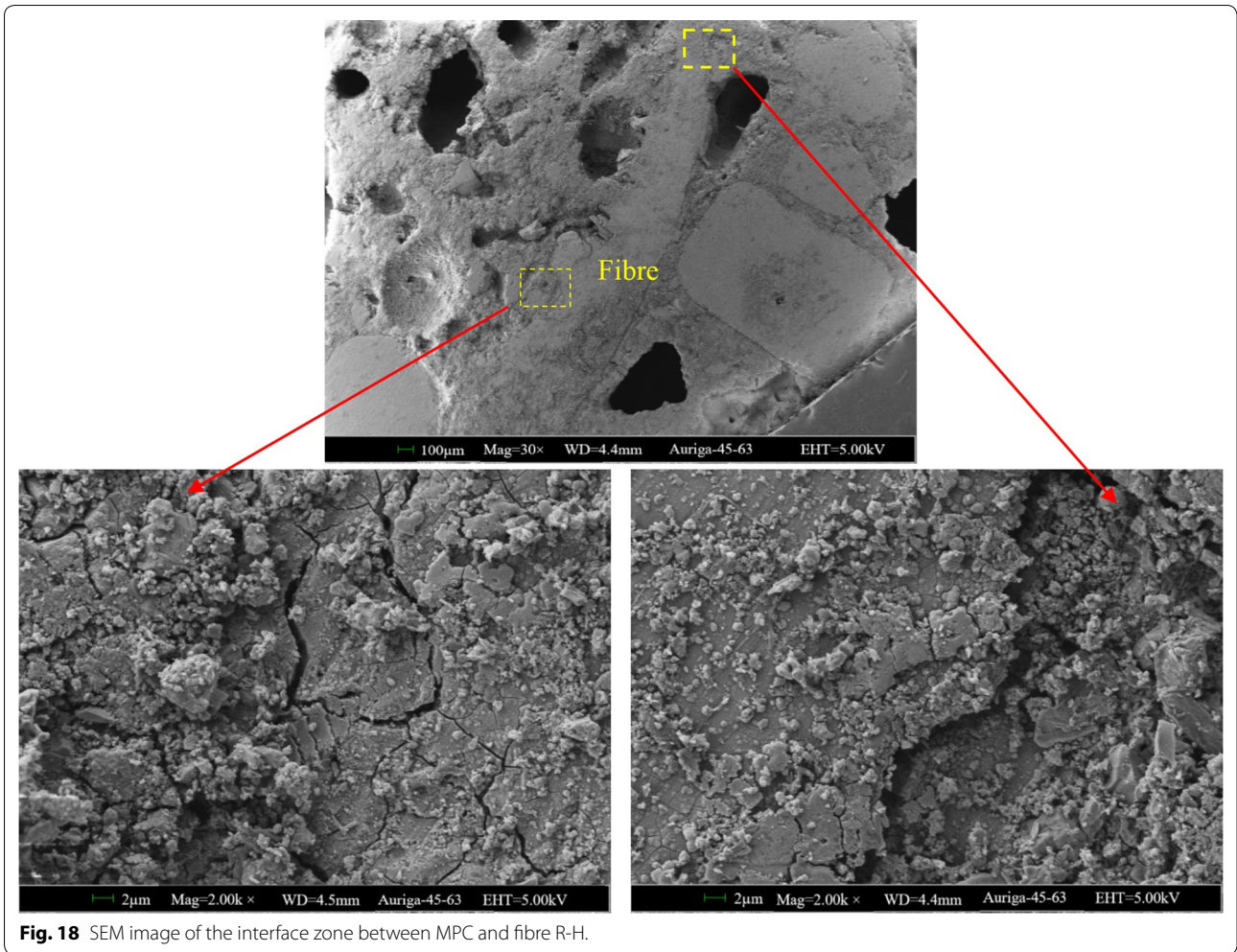


**Fig. 17** SEM image of the interface zone between MPC and fibre S-2.



caused the matrix surrounding the fibre to split and then to break (Fig. 15). However, the ratio of material use of I-A fibre was limited to only 43.9% due to the matrix

breakage. Based on the average bond strength of straight fibre (S-2) without coating, the physicochemical and mechanical contributions for the pullout load of I-A fibre

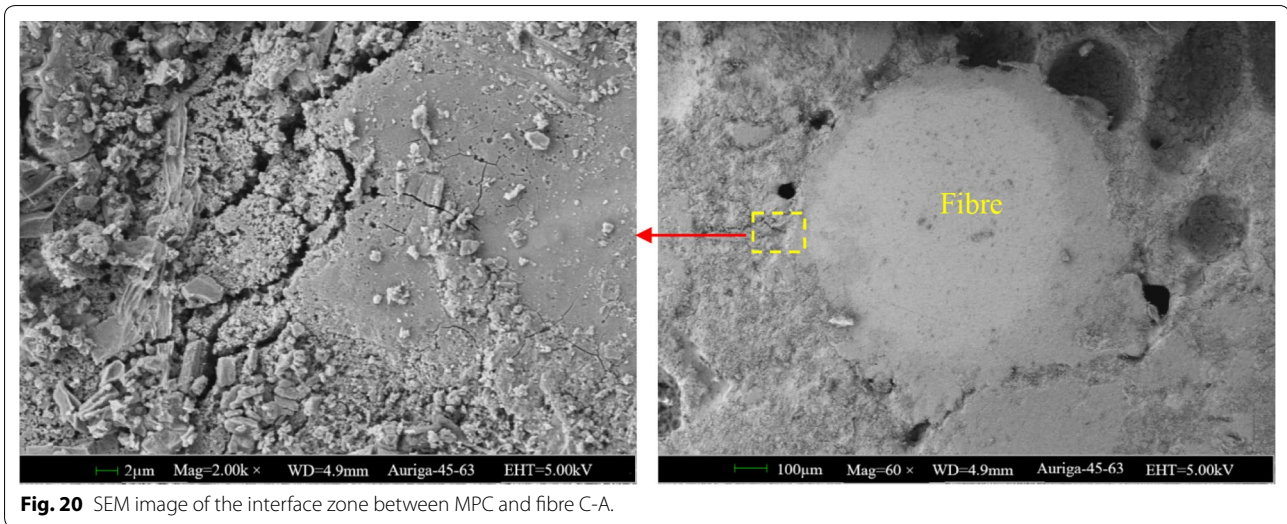


**Fig. 20** SEM image of the interface zone between MPC and fibre C-A.

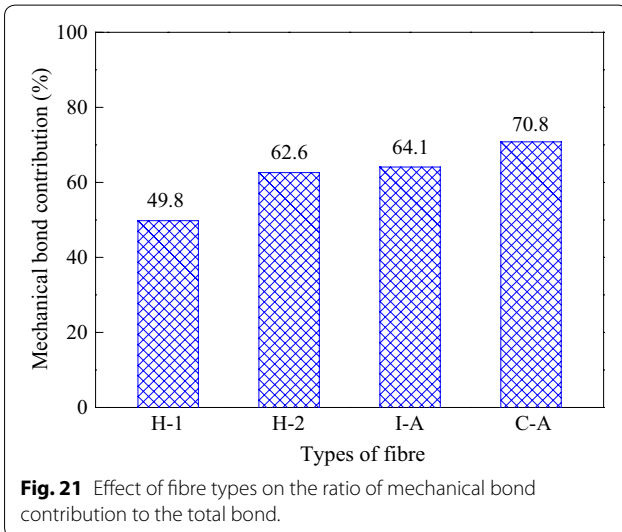


**Fig. 21** Effect of fibre types on the ratio of mechanical bond contribution to the total bond.

were calculated as 244.0 N and 435.6 N, respectively. The ratios of the physicochemical bond and mechanical bond contributions to the total bond were 35.9% and 64.1%, respectively.

#### 4.4 Interface Transition Zone Between MPC and Varies Fibres

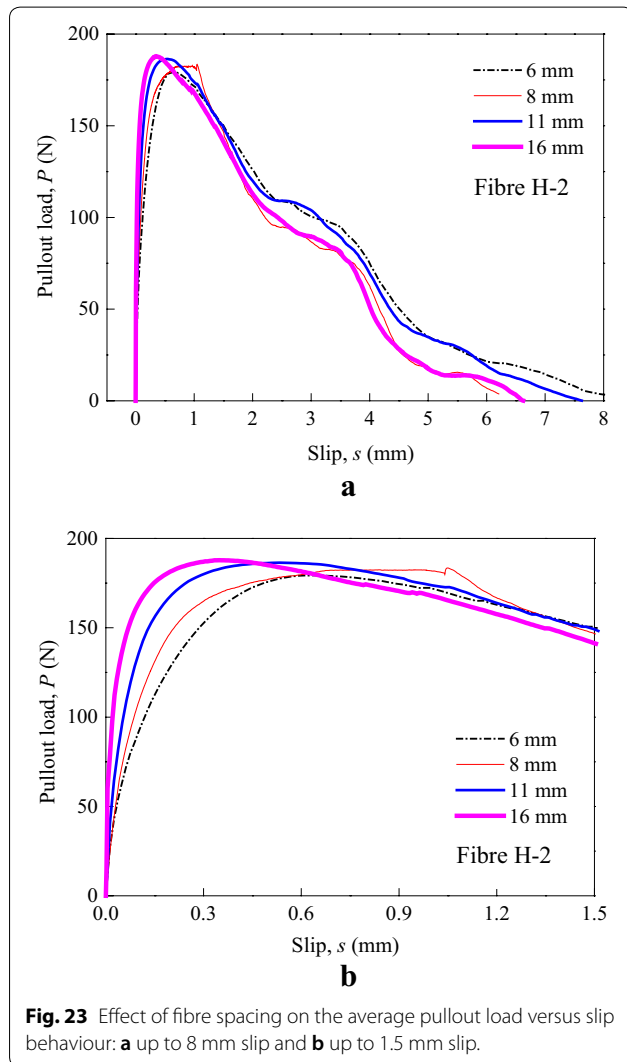
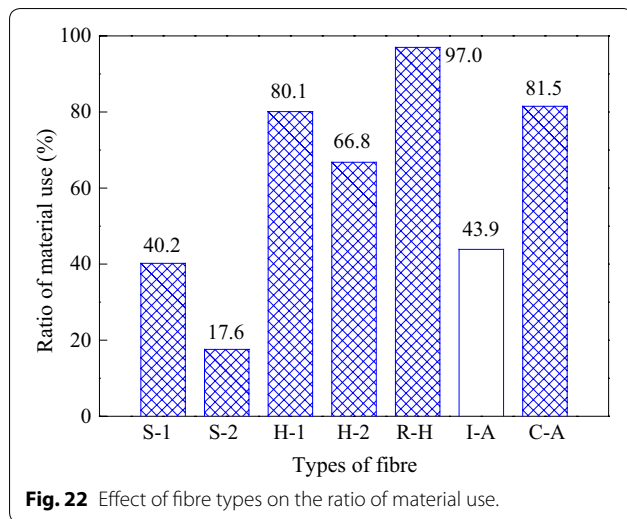
The micromorphology of the interface zone between MPC and different types of fibres was examined by field emission scanning electron microscope (Zeiss, Auriga FIB, Germany). The S-1 and S-2 fibres are straight. The H-1 and H-2 fibres are hooked at the ends. However, the material and surface of fibre S-1 are the same as the material and surface of fibre H-1. The material and surface of fibre S-2 are the same as the material and surface

of fibre H-2. Hence, the specimens with H-1 and H-2 fibres were not examined. Figures 16, 17, 18, 19 and 20 present the SEM micrograph of the interface transition zone between MPC and fibres: S-1, S-2, R-H, I-A, and C-A, respectively.

It was found that, for case of S-1 fibre, the interface zone was the most compact and most flawless. The average bond strength between S-1 fibre and MPC matrix was the highest. In comparison to S-1 fibre, the interface zone between S-2 fibre and MPC was less compact. Also, there were some micro-defects less than 1 µm in the interface zone between S-2 fibre and MPC. In comparison to S-2 fibre, the interface zone between R-H fibre and MPC was less compact. However, the bump of the roughened surface of R-H fibre increased the contact area between the fibre and matrix, which improved the bond between fibre and matrix. There were some micro-defects of about 2 µm in the interface zone between I-A fibre and MPC. The larger equivalent diameter of I-A fibre caused more micro-defects in the interface. It indicated that the physicochemical bond between I-A fibre and MPC was weaker compared to the other fibres. The mechanical bond contributed most to the bond between I-A fibre and MPC. The interface zone between C-A fibre and MPC was similar with that between S-2 fibre and MPC. However, the interface zone between C-A fibre and MPC, with less micro-defect, was slightly less compact. It indicated that the average bond strengths of C-A and S-2 fibres were similar.

#### 4.5 Summary of the Effect of Different Types of Fibre

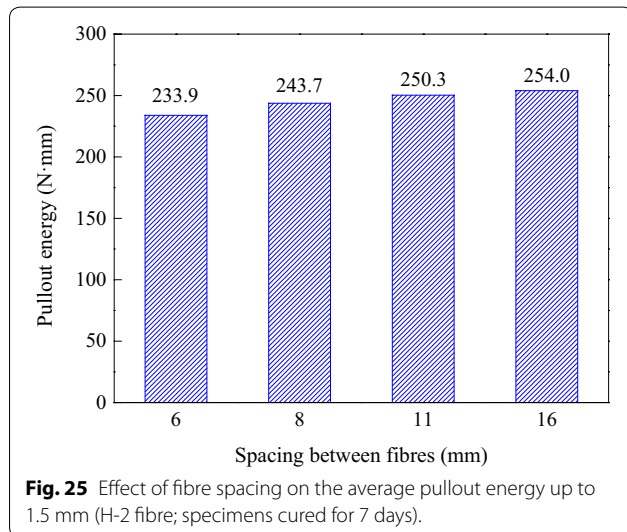
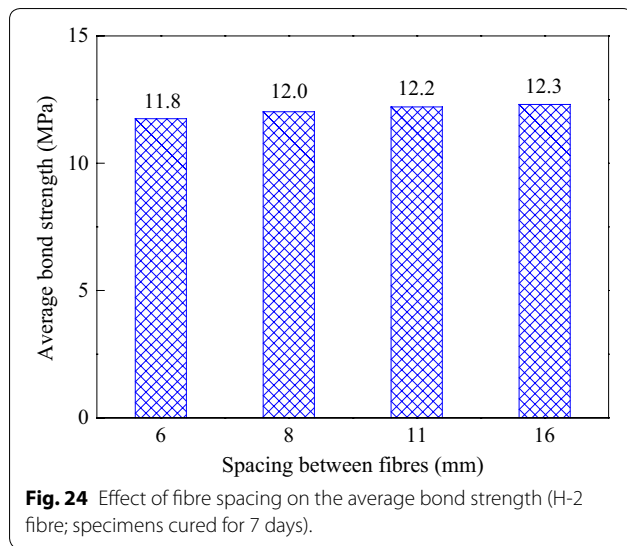
Figure 21 summarizes the ratio of mechanical bond contribution of various fibres. The order of the ratio of the mechanical bond contribution to total bond for various



fibres was: C-A (70.8%), I-A (64.1%), H-2 (62.6%) and H-1 (49.8%). The ratio of the mechanical bond contribution of C-A and I-A fibres was larger than that for H-2 and H-1 fibres. The end hook deformation provided the mechanical bond locally, which caused a significant mechanical bond. The deformations (crimp and indentation) along the length of the fibre provided the mechanical bond distributed along the fibre which caused significantly higher mechanical bond. Figure 22 summarizes the ratio of material use with various fibres. The order of the ratio of material use for various fibres was: R-H (97%), C-A (81.5%), H-1 (80.1%), H-2 (66.8%), I-A (43.9%), S-1 (40.2%) and S-2 (17.6%). The ratio of material use for R-H fibre was the highest, followed by C-A, H-1 and H-2 fibre. The ratio of material use for the straight fibre (S-1 and S-2) was the lowest. The end-hook deformation significantly improved the ratio of material use of fibres. The roughened surface and deformations (crimped and indented) along fibre length improved the ratio of material use of fibre more significantly. The order of average bond strength for various fibres was: C-A (15.0 MPa), R-H (14.7 MPa), I-A (12.5 MPa), H-2 (12.0 MPa), H-1 (10.5 MPa), S-1 (7.0 MPa) and S-2 (4.5 MPa), as shown in Fig. 11. The average bond strength for C-A and R-H fibre was the highest, followed by I-A, H-2 and H-1 fibre. The average bond strength for the straight fibre (S-1 and S-2) was the lowest. The end-hook deformation significantly improved the average bond strength. However, the rough surface and deformation along fibre length improved the average bond strength more significantly. It is noted that the effectiveness of I-A fibre is limited by the low ratio of material use due to the matrix fracture during the pullout process. The order of pullout energy per unit volume for various fibres was: H-1 (530.5 N mm/mm<sup>3</sup>), S-1 (300.2 N mm/mm<sup>3</sup>), H-2 (173.1 N mm/mm<sup>3</sup>), C-A (115.1 N mm/mm<sup>3</sup>), R-H (105.1 N mm/mm<sup>3</sup>), I-A (68.0 N mm/mm<sup>3</sup>) and S-2 (53.3 N mm/mm<sup>3</sup>), as shown in Fig. 12. The pullout energy per unit volume of C-A, R-H and I-A fibres was lower than that of the hooked-end fibres (H-1 and H-2) due to the larger cross-sectional area of C-A, R-H and I-A fibres.

#### 4.6 Failure Modes of Pullout Steel Fibres Embedded in the MPC-Based Matrix

In a previous study conducted by the authors, the pullout half of the specimens prepared with MPC fractured along the cross-section perpendicular to the fibre during the hooked-end fibre (H-2) pullout test (Feng et al. 2018). It was caused by the low tensile strength of the matrix cured for 6 h. During the pullout process of I-A fibre, the transverse tensile stress contributed by the surface indentation of the fibre was relatively high. Hence, the matrix surrounding fibres



failed due to splitting. The material use of the fibre was limited to a low level in this failure mode. The average bond strength of R-H fibre was high due to the surface

roughness and end-hook. The tensile stress in R-H fibre easily reached the tensile strength of the fibre. Hence, the R-H fibre failed during the pullout process. However, the other fibres (S-1, S-2, H-1, H-2 and C-A), during the pullout process, were pulled out from the MPC-base matrix (no failure of fibres and matrix) in this study. According to the test results of the previous and present studies, the failure mode of pullout steel fibre embedded in the MPC-based matrix can be summarized as follows: (1) fibre pull out (S-1, S-2, H-1, H-2 and C-A fibres), (2) fibre failure (R-H fibre), (3) matrix splitting surrounding the fibre (I-A fibre) and (4) matrix fracture perpendicular to the fibre length at the cross-section. The failure mode is determined by the mechanical properties of the matrix (such as strength and packing density) and properties of the steel fibres (surface properties, such as smooth, etched or roughened; deformations at fibre ends, such as paddles, buttons or hooks; and deformation along the fibre length, such as in crimped, indented or polygonal twisted fibres).

**4.7 Group Effect of Steel Fibre on the Pullout Behaviour**

The pullout tests with varying spacing and number of fibres were carried out to investigate the group effect of the steel fibres embedded in the MPC-based matrix. Figure 23 summarizes the pullout load–slip curves of H-2 fibre with varying fibre spacing. Figures 24 and 25 present the average bond strength and pullout energy per unit volume of H-2 fibre, respectively, with varying fibres spacing. Table 5 summarizes the pullout parameters with varying fibre spacing. The relative spacing is defined as the spacing of the fibres divided by the embedment length of the fibres.

It can be observed that the maximum pullout load during the pullout process slightly decreased with the decrease in the fibre spacing from 16 to 6 mm (relative spacing from 1.78 to 0.67), as shown in Fig. 23. The average bond strength also slightly decreased with the decrease in the fibre spacing from 16 to 6 mm (relative spacing from 1.78 to 0.67), as shown in Fig. 24. The

**Table 5** Pullout parameters derived from test results with different fibre spacing.

Type of fibre	Compressive strength of matrix (MPa)	Spacing of fibres (mm)	Relative spacing	Maximum pullout load (N)	Maximum fibre tensile stress (MPa)	Average bond strength (MPa)	Pullout energy (N mm)	
							Up to 2.5 mm	Up to 1.5 mm
H-2	37.4	16	1.78	187.8	820.6	12.3	368.0	254.0
		11	1.22	183.5	801.5	12.2	375.2	250.3
		8	0.89	183.4	801.4	12.0	356.6	243.7
		6	0.67	179.3	783.3	11.8	360.7	233.9

The reported values are the average values of the test results.

The relative spacing is defined as the spacing of the fibres divided by the embedment length of the fibres.

pullout energy,  $W_p$ , calculated by Eq. 4, slightly fluctuated with the change of the fibre spacing from 6 to 16 mm, as shown in Table 5. However, the pullout energy per unit volume,  $W_p$ , determined up to 1.5 mm slip, slightly decreased with the decrease in the fibre spacing from 16 to 6 mm (relative spacing from 1.78 to 0.67), as shown in Fig. 25. It revealed that the group effect of the fibres weakened the bond between the steel fibres and MPC-based matrix when the relative spacing of the fibres changed from 1.78 to 0.67. The group effect could be more significant in the composites with a large volume fraction of fibres with a small fibre spacing. The group effect for composites with a large volume fraction of fibre might reduce the fibre efficiency presented in this study.

## 5 Conclusions

The effect of seven types of steel fibres on the pullout behaviour of steel fibre embedded in the MPC-based matrix was experimentally investigated. The group effect of the fibres on the pullout behaviour of steel fibre embedded in the MPC-based matrix was also explored. The experimental results have led to the following conclusions:

1. The lower stressing to the matrix and the damaged surface helped in maintaining a higher pullout resistance during the pullout test for the smaller diameter steel fibres with brass coating surface. The smaller diameter steel fibres with brass coating surface showed a more efficient crack-bridging behaviour in the MPC-based matrix. The efficient crack-bridging behaviour was reflected in higher average bond strength, higher pullout energy per unit volume and a higher ratio of material use.
2. The ratio of the mechanical bond contribution of the fibres with deformation along the length of the fibre was higher than the ratio of the mechanical bond contribution of the hooked end fibre. The end hook deformation provided mechanical bond locally, which significantly increased the ratio of materials use, average bond strength and pullout energy. The deformations along the length of the fibre provided mechanical bond distributed along the fibre, which increased the ratio of materials use and average bond strength more significantly.
3. The failure mode of the pullout steel fibre embedded in the MPC-based matrix is determined by the surface roughness of the fibre, deformations at the fibre end and along the length of the fibre, and the mechanical properties of the matrix. The failure mode can be characterized into: fibre pullout (S-1, S-2, H-1, H-2 and C-A fibres), fibre failure (R-H fibre), matrix splitting surround the fibre (I-A fibre),

and matrix fracture perpendicular to the length of the fibre at the cross-section.

4. The maximum of pullout load, fibre tensile stress, average bond strength, and pullout energy per unit volume slightly decreased with the decrease of the relative spacing of fibres from 1.78 to 0.67. The group effect of the fibres weakened the bond between the steel fibres and MPC-based matrix when the relative spacing of the fibres changed from 1.78 to 0.67.

### Authors' contributions

HF was a major contributor in the design of the study and collection, analysis, and interpretation of data and in writing the manuscript. MNS and MNSH analyzed the results of the experiment and improved the writing of the manuscript. LF operated the experiment and summed up the test data. DG and JZ improved the experimental program and interpreted the test data of the experiment. All authors read and approved the final manuscript.

### Author details

<sup>1</sup> School of Civil Engineering, Zhengzhou University, Zhengzhou, Henan 450001, China. <sup>2</sup> School of Civil, Mining and Environmental Engineering, University of Wollongong, Wollongong, NSW 2522, Australia. <sup>3</sup> Yellow River Engineering Consulting Co., Ltd., Zhengzhou, Henan 450003, China.

### Acknowledgements

The authors acknowledge the University of Wollongong, Australia for providing research foundation. The first author would like to acknowledge the University of Wollongong, Australia, and the China Scholarship Council for supporting his overseas research scholarship.

### Competing interests

The authors declare that they have no competing interests.

### Availability of data and materials

The datasets used and analysed during the current study are available from the corresponding author on reasonable request.

### Funding

This work was financially supported by the National Key R&D Program of China (2016YFE0125600), National Natural Science Foundation of China (Grant No. 51308504), and Program of Young-backbone-teachers in University of Henan Province of China (2016GGJS-005).

### Publisher's Note

Springer Nature remains neutral with regard to jurisdictional claims in published maps and institutional affiliations.

Received: 20 November 2018 Accepted: 2 April 2019

Published online: 01 May 2019

### References

- Abdelrazig, B. E. I., & Sharp, J. H. (1985). A discussion of the papers on magnesia-phosphate cements b. *Cement and Concrete Research*, 15(5), 921–922.
- Abdelrazig, B. E. I., Sharp, J. H., & El-Jazairi, B. (1988). The chemical composition of mortars made from magnesia-phosphate cement. *Cement and Concrete Research*, 18(3), 415–425.
- Abdelrazig, B. E. I., Sharp, J. H., & El-Jazairi, B. (1989). The microstructure and mechanical properties of mortars made from magnesia-phosphate cement. *Cement and Concrete Research*, 19(2), 247–258.
- ASTM C109/C109M-16a. (2016). *Standard test method for compressive strength of hydraulic cement mortars (using 2-in. or [50-mm] cube specimens)*. West Conshohocken: ASTM International. <http://www.astm.org>.
- Banda Technology Co., Ltd. of Liaoning, China. Retrieved November 2018 from <http://www.lnpdkj.com/>. (in Chinese).

- Banthia, N., & Sheng, J. (1990). Micro-reinforced cementitious materials. In *MRS Online Proceedings Library* (vol. 211, pp. 25).
- Banthia, N., & Trottier, J. F. (1995). Concrete reinforced with deformed steel fibers part II: toughness characterization. *ACI Materials Journal*, 92(2), 146–154.
- Bekaert China Co., Ltd. Shanghai, China. Retrieved November 2018 from <https://www.bekaert.com.cn/>. (in Chinese).
- Betterman, L. R., Ouyang, C., & Shah, S. P. (1995). Fiber–matrix interaction in microfiber reinforced mortar. *Advanced Cement Based Materials*, 2(2), 53–61.
- Chan, Y. W., & Chu, S. H. (2004). Effect of silica fume on steel fiber bond characteristics in reactive powder concrete. *Cement and Concrete Research*, 34(7), 1167–1172.
- Cunha, V. M. C. F., Barros, J. A. O., & Sena-Cruz, J. M. (2010). Pullout behavior of steel fibers in self-compacting concrete. *Journal of Materials in Civil Engineering ASCE*, 22(1), 1–9.
- Ezeldin, A., & Balaguru, P. (1992). Toughness behavior of fiber reinforced rapid set materials: A preliminary study. *ASTM Journal, Cement, Concrete, and Aggregates*, 14(1), 3–7.
- Feng, H., Neaz Sheikh, M., Hadi, M. N. S., Feng, L., Gao, D., & Zhao, J. (2018a). Interface bond performance of steel fibre embedded in magnesium phosphate cementitious composite. *Construction and Building Materials*, 185, 648–660.
- Feng, H., Neaz Sheikh, M., Hadi, M. N. S., Gao, D., & Zhao, J. (2018b). Mechanical properties of micro-steel fibre reinforced magnesium potassium phosphate cement composite. *Construction and Building Materials*, 185, 423–435.
- Frantzis, P., & Baggott, R. (2000). Bond between reinforcing steel fibres and magnesium phosphate/calcium aluminate binders. *Cement and Concrete Composites*, 22(3), 187–192.
- Frantzis, P., & Baggott, R. (2003). Transition points in steel fiber pullout tests from magnesium phosphate and accelerated calcium aluminates binders. *Cement and Concrete Composites*, 25(1), 11–17.
- Hall, D. A., Stevens, R., & El-Jazairi, B. (2001). The effect of retarders on the micro-structure and mechanical properties of magnesia-phosphate cement mortar. *Cement and Concrete Research*, 31(3), 455–465.
- Helfet, J. L., & Harris, B. (1972). Fracture toughness of composites reinforced with discontinuous fibers. *Journal of Materials Science*, 7(5), 494–498.
- JCI SF-8. (2002). *Method of test for bond of fibers*. Tokyo: Japan Concrete Institute.
- Kermel Chemical Reagent Co., Ltd. Tianjin, China. Retrieved November 2018 from <http://www.tjkermel.com/>. (in Chinese).
- Kim, D., El-Tawil, S., & Naaman, A. E. (2008). Loading rate effect on pullout behavior of deformed steel fibers. *ACI Materials Journal*, 105(6), 576–584.
- Li, V. C., Wang, Y., & Backer, S. (1990). Effect of inclining angle, bundling and surface treatment on synthetic fibre pull-out from a cement matrix. *Composites*, 21(2), 132–140.
- Naaman, A. E., & Najm, H. (1991). Bond-slip mechanisms of steel fibers in concrete. *ACI Materials Journal*, 88(2), 135–145.
- Naaman, A. E., & Shah, S. P. (1976). Pull-out mechanism in steel fiber-reinforced concrete. *ASCE Journal of the Structural Division*, 102(8), 1537–1548.
- Ohama, Y., Miyara, M., & Endo, M. (1985). Properties of steel fiber and polyethylene fiber hybrid reinforced polymer-modified concrete. In *The Twenty-eighth Japan Congress on Materials Research* (pp. 151–156). Kyoto, Japan: The Society of Materials Science.
- Peled, A., Guttman, H., & Bentur, A. (1992). Treatments of polypropylene fibres to optimize their reinforcing efficiency in cement composites. *Cement and Concrete Composites*, 14(4), 277–285.
- Péra, J., & Ambroise, J. (1998). Fiber-reinforced magnesia-phosphate cement composites for rapid repair. *Cement and Concrete Composites*, 20(1), 31–39.
- Ramakrishnan, V., Brandshaug, T., Coyle, W. V., & Schrader, E. K. (1980). A comparative evaluation of concrete reinforced with straight steel fibers and fibers with deformed ends glued together into bundles. *ACI Journal Proceedings*, 77(3), 135–143.
- Robins, P., Austin, S., & Jones, P. (2002). Pull-out behaviour of hooked steel fibres. *Materials and Structures*, 35, 434–442.
- Rossi, P., & Harrouche, N. (1990). Mix design and mechanical behaviour of some steel fibre-reinforced concretes used in reinforced concrete structures. *Materials and Structures*, 23(4), 256–266.
- Roy, D. M. (1987). New strong cement materials: chemically bonded ceramics. *Science*, 235(4789), 651–658.
- Shanghai Harex Steel Fiber Technology Co., Ltd. 458 Laodong Road, Jiading, Shanghai, China. Retrieved November 2018 from <http://www.shhar.com/page/7.htm>. (in Chinese).
- Shanghai Realstrong Steel Fibre Co., Ltd. 365 Wang Ln, Jinze Town, Shanghai, China. Retrieved November 2018 from <http://www.realstrong.cn/cn/product151.asp>. (in Chinese).
- Shannag, M. J., Brincker, R., & Hansen, W. (1997). Pullout behavior of steel fibers from cement-based composites. *Cement and Concrete Research*, 27(6), 925–936.
- Stähli, P., Custer, R., & van Mier, J. M. (2008). On flow properties, fibre distribution, fibre orientation and flexural behaviour of FRC. *Materials and Structures*, 41(1), 189–196.
- Sugama, T., & Kukacka, L. E. (1983). Magnesium monophosphate cements derived from diammonium phosphate solutions. *Cement and Concrete Research*, 13(3), 407–416.
- Weitong Chemical Co., Ltd of Wujiang, Jiangsu, China. Retrieved November 2018 from <https://wjwthg1818.1688.com/>. (in Chinese).
- Wille, K., & Naaman, A. E. (2012). Pullout behavior of high-strength steel fibers embedded in ultra-high-performance concrete. *ACI Materials Journal*, 109(4), 479–487.
- Yang, Q. B., & Wu, X. L. (1999). Factors influencing properties of phosphate cement-based binder for rapid repair of concrete. *Cement and Concrete Research*, 29(3), 389–396.
- Yang, Q. B., Zhang, S., & Wu, X. (2002). Deicer-scaling resistance of phosphate cement based binder for rapid repair of concrete. *Cement and Concrete Research*, 32, 165–168.
- Yang, Q. B., Zhu, B., & Wu, X. (2000a). Characteristics and durability test of magnesium phosphate cement-based material for rapid repair of concrete. *Materials and Structures*, 33(4), 229–234.
- Yang, Q. B., Zhu, B., Zhang, S., & Wu, X. (2000b). Properties and applications of magnesia phosphate cement mortar for rapid repair of concrete. *Cement and Concrete Research*, 30(11), 1807–1813.
- Zhengyang Casting Material Company. Xinmi, Henan, China. Retrieved November 2018 from <http://www.igreenbuy.com/index.php/shop-info-2728.html/>. (in Chinese).
- Zhengzhou YuJian Steel Fiber Co., Ltd. Building 2, 1105 Xuefu Square, Zhengdong New District, Zhengzhou City, Henan, China. Retrieved November 2018 from <http://www.zzyujian.com/>. (in Chinese).
- Zhitai Steel Fiber Co., Ltd. Yahong Bridge, Yutian, Hebei, China. Retrieved November 2018 from <http://www.ztgxw.cn/>. (in Chinese).

Submit your manuscript to a SpringerOpen® journal and benefit from:

- Convenient online submission
- Rigorous peer review
- Open access: articles freely available online
- High visibility within the field
- Retaining the copyright to your article

Submit your next manuscript at ► [springeropen.com](http://springeropen.com)